Organic Geochemistry 41 (2010) 1285–1296

Contents lists available at ScienceDirect

Organic Geochemistry

journal homepage: www.elsevier.com/locate/orggeochem

Carbon and hydrogen isotopic reversals in deep basin gas: Evidence for limits to the stability of hydrocarbons

R.C. Burruss [a,*], C.D. Laughrey [b,1]

[a] US Geological Survey, National Center MS956, 12201 Sunrise Valley Drive, Reston, VA 20192, United States
[b] Pennsylvania Department of Conservation and Natural Resources, Bureau of Topographic and Geologic Survey, 400 Waterfront Drive, Pittsburgh, PA 15222, United States

ARTICLE INFO

Article history:
Received 19 April 2010
Received in revised form 14 September 2010
Accepted 17 September 2010
Available online 24 September 2010

ABSTRACT

During studies of unconventional natural gas reservoirs of Silurian and Ordovician age in the northern Appalachian basin we observed complete reversal of the normal trend of carbon isotopic composition, such that $\delta^{13}C$ methane (C_1) >$\delta^{13}C$ ethane (C_2) >$\delta^{13}C$ propane (C_3). In addition, we have observed isotopic reversals in the δ^2H in the deepest samples. Isotopic reversals cannot be explained by current models of hydrocarbon gas generation. Previous observations of partial isotopic reversals have been explained by mixing between gases from different sources and thermal maturities. We have constructed a model which, in addition to mixing, requires Rayleigh fractionation of C_2 and C_3 to cause enrichment in ^{13}C and create reversals. In the deepest samples, the normal trend of increasing enrichment of ^{13}C and ^2H in methane with increasing depth reverses and ^2H becomes depleted as ^{13}C becomes enriched. We propose that the reactions that drive Rayleigh fractionation of C_2 and C_3 involve redox reactions with transition metals and water at late stages of catagenesis at temperatures on the order of 250–300 °C. Published *ab initio* calculated fractionation factors for C–C bond breaking in ethane at these temperatures are consistent with our observations. The reversed trend in δ^2H in methane appears to be caused by isotopic exchange with formation water at the same temperatures. Our interpretation that Rayleigh fractionation during redox reactions is causing isotopic reversals has important implications for natural gas resources in deeply buried sedimentary basins.

Published by Elsevier Ltd.

1. Introduction

Natural gas is the cleanest, least carbon intensive fossil fuel. Increasing demand for natural gas has lead to discovery and exploitation of a range of unconventional gas accumulations such as basin center gas, tight gas sands, fractured reservoirs, coalbed methane and shale gas. Our concepts of the geochemistry of the origin and distribution of hydrocarbon gases are based on many years of empirical observations (Schoell, 1983), laboratory experiments (Behar et al., 1992; Berner et al., 1995; Lorant et al., 1998) and theoretical modeling (James, 1983; Chung et al., 1988; Rooney et al., 1995; Tang et al., 2000) of systematic variations in molecular and carbon and hydrogen isotopic compositions as a function of thermal maturity in deep basins or microbial processes at shallow depths. Most field and laboratory observations and all theoretical models of kinetic isotope effects (KIEs) yield a normal sequence of carbon isotopic compositions with $\delta^{13}C$ methane (C_1) <$\delta^{13}C$ ethane (C_2) <$\delta^{13}C$ propane (C_3) and <$\delta^{13}C$ butane (C_4) observed in natural gas accumulations worldwide.

As exploration has shifted to unconventional gas accumulations, a small number of studies (Jenden et al., 1993; Laughrey and Baldassare, 1998; Burruss and Ryder, 2003) have begun to report reversals in the normal sequence of isotopic compositions. Most previous studies report partial reversals in which $\delta^{13}C_1 > \delta^{13}C_2$ or $\delta^{13}C_2 > \delta^{13}C_3$. During studies on gas accumulations in tight gas sandstone (Burruss and Ryder, 2003) and fractured hydrothermal dolomite reservoirs in the northern Appalachian Basin, USA, (Laughrey and Kostelnik, 2007) we discovered that all reservoirs with present day depths >3 km have hydrocarbon gases with $\delta^{13}C$ fully reversed such that $\delta^{13}C_1 > \delta^{13}C_2 > \delta^{13}C_3$ and in some of the deepest samples, the hydrogen isotopic compositions (δ^2H) of C_1 and C_2 are also reversed.

Current models of hydrocarbon gas generation cannot explain the isotopic reversals we observe in the Appalachian Basin. Previous work described the origin of partial isotopic reversals by mixing between gases from different sources, including abiotic sources, and sources at different levels of thermal maturity (Jenden et al., 1993; Dai et al., 2004; Huang et al., 2004). Observations of partial reversals in gases from mineral exploration boreholes in

* Corresponding author. Tel.: +1 703 648 6144.
E-mail addresses: burruss@usgs.gov (R.C. Burruss), christopher.laughrey@weatherfordlabs.com (C.D. Laughrey).
[1] Present address: Weatherford Laboratories, Unconventional Reservoir Services, 16161 Table Mountain Parkway, Golden, CO 80403, United States. Tel.: +1 720 898 8200.

0146-6380/$ - see front matter Published by Elsevier Ltd.
doi:10.1016/j.orggeochem.2010.09.008

crystalline Precambrian rocks (Sherwood Lollar et al., 2002, 2006) and in gases discharging from onshore and offshore geothermal systems (Des Marais et al., 1981; Proskurowski et al., 2008) has raised the possibility of an abiotic source from mineral catalyzed reduction of CO_2 with H_2 or polymerization of CH_4 (Sherwood Lollar et al., 2002, 2008). It is also known that oxidative destruction of hydrocarbon gases either microbially (James and Burns, 1984; Chung et al., 1988) or by thermochemical sulfate reduction (Krouse et al., 1988) can lead to partial reversals in isotopic composition.

In this paper we describe the stable isotope geochemistry of natural gases in reservoirs within lower Paleozoic strata of the northern Appalachian Basin. We explain the origin of the isotopic reversals in the deepest samples with a model that includes mixing of gases, Rayleigh-type fractionation of the isotopic compositions of C_2 and C_3, and late stage generation of methane during maximum burial. High temperatures and mineral-fluid reactions during maximum burial appear to have been high enough to cause isotopic exchange between CH_4 and H_2O, leading to reversals in isotopic trends with depth and the δ^2H reversal between C_1 and C_2. Simultaneous reversals in $\delta^{13}C$ and δ^2H between hydrocarbon gases may be an important signal of limits to stability of hydrocarbon gases in deep basins. If our interpretation is correct, then observation of isotopic reversals during exploration of unconventional natural gas plays may be an indicator of the possibility that the play is approaching the maximum limit of stability of hydrocarbons in the basin.

2. Geologic setting and samples

2.1. Geologic setting

2.1.1. Petroleum geology

The principal gas-producing region of the north and central Appalachian foreland basin (Fig. 1) encompasses a broad area between the structural Allegheny front on the east, the Cincinnati and other contiguous arches on the west, the Canadian shield on the north and a somewhat ambiguous boundary on the south where the basin narrows between the Pine Mountain thrust and the Nashville Dome in northern Tennessee and southern Kentucky (Schumaker, 1996). The rocks within this area are relatively undeformed; structures consist of detached folded rocks above buried, blind thrusts in the eastern portion of the foreland basin, west of the Allegheny front, in West Virginia, Maryland and Pennsylvania. Folding decreases west and northwest from the front into New York, Ohio, Kentucky and Tennessee until the northwest flank of the Appalachian Basin becomes a gently south-eastward dipping homocline. Significantly deformed sedimentary rocks of the Ridge and Valley and Great Valley physiographic provinces, which lie between the Precambrian rocks of the Blue Ridge and the Allegheny front, comprise the Appalachian thrust belt. Rocks of the thrust belt extend along the full length of the Appalachian orogen, but only produce minor amounts of natural gas. Three major tectonic events

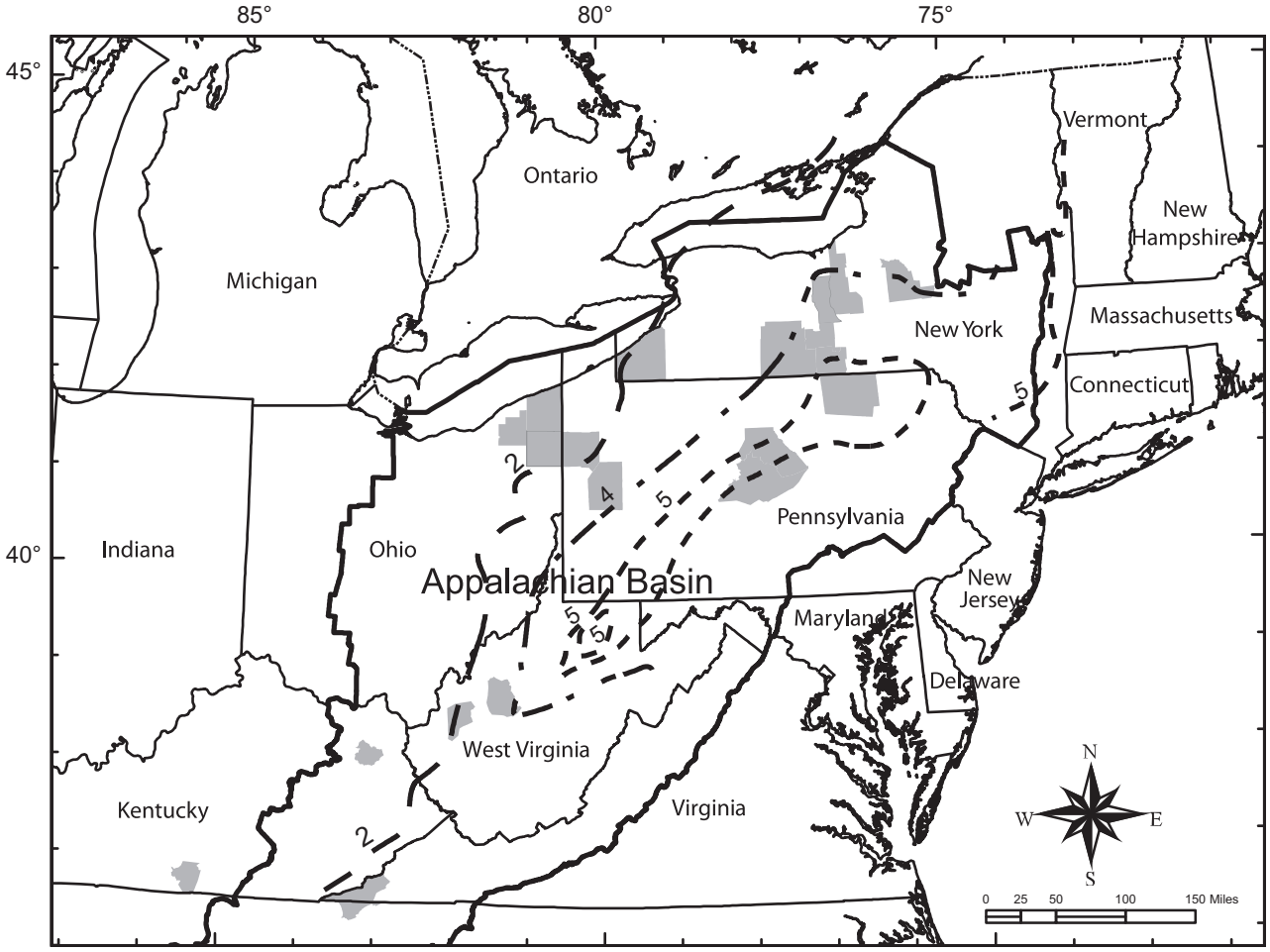

Fig. 1. Map of the geographic distribution and thermal maturity of sampled reservoirs. The map of the northern Appalachian basin (solid black outline) shows contours of conodont alteration index (thermal maturity) within Ordovician age rocks as dashed lines that are simplified from published maps in Repetski et al. (2008). Gas samples were obtained from fields within the counties shown in light gray. Non-associated gases (NAG) occur in fields within the area of conodont alteration indices (CAI) greater than 4 (maximum paleotemperature about 200 °C) including samples from areas with CAI > 5 (maximum paleotemperature >250 °C).

created or influenced structures in the Appalachian basin: the Grenville orogeny (~900 Ma); Iapetian rifting (~570 Ma); and the Alleghanian orogeny (~275 Ma). The Grenville orogeny and Iapetian rifting predate the formation of the Appalachian foreland basin, but reactivation of basement structures formed during these earlier deformations influenced most subsequent geologic events, including the distribution of petroleum in the basin (Schumaker, 1996).

With the exception of widely scattered, small and localized igneous intrusions of Mesozoic age, all of the rocks of the Appalachian foreland basin consist of Paleozoic sediments. The lithostratigraphic successions of the Appalachian Basin are comprised of a variety of carbonates, evaporates and siliciclastic rocks ranging in age from Cambrian to Permian (Fig. 2). Numerous regional coal beds are important in Pennsylvanian and, to a lesser extent, in Mississippian and Devonian rocks. Quaternary glacial deposits are largely restricted to the northern portions of the basin. The Paleozoic rocks of the Appalachian Basin overlie a Precambrian basement that consists of highly metamorphosed rocks of the Grenville Province.

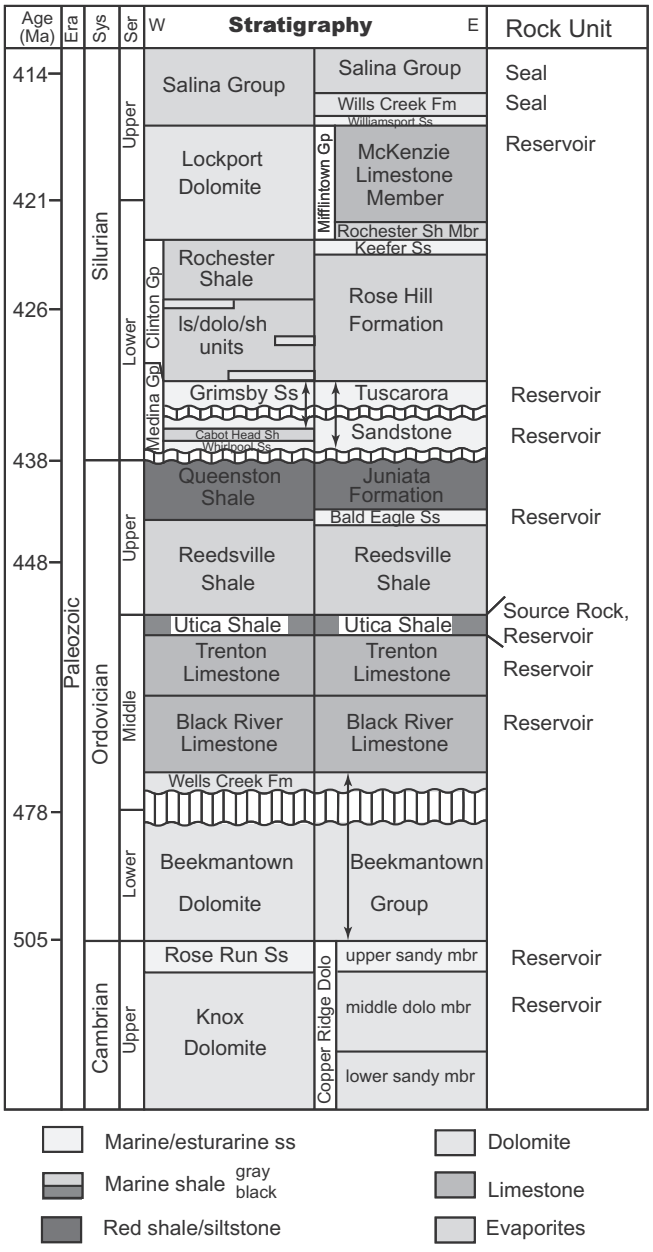

Fig. 2. Stratigraphic column for the study area. Intervals of source rocks, reservoirs, and seals for the gases in this study are indicated.

The hydrocarbons analyzed in this study were generated from organic matter in the Utica Formation of Middle Ordovician age and its stratigraphic equivalents, the Antes, and Point Pleasant shales (Fig. 2, Ryder et al., 1998; Swezey, 2002). Sedimentary organic matter in rocks of this age is commonly enriched in the remains of the organism *Gloeocapsamorpha prisca* (*G. prisca*) which can have $\delta^{13}C = -34‰$ to $-26‰$ (Hatch et al., 1987; Mastalerz et al., 2003). Hydrocarbons generated from rocks rich in *G. prisca* have a similar range of isotopic compositions (Hatch et al., 1987). Present day total organic carbon (TOC) in the Utica, Antes and Point Pleasant shales averages 1.8% and the genetic potential averages 6.4 mgHC/g rock (Ryder et al., 1998). The shales cover an area of ~106,149 km^2 in the basin. The Utica, Antes and Point Pleasant shales are mature with respect to oil throughout central and eastern Ohio and become post mature down dip into Pennsylvania, New York and West Virginia (Rowan, 2006). These rocks are exploited as thermogenic shale gas reservoirs in Ohio, Pennsylvania and New York.

Most of the lower Palaeozoic gas samples we discuss in this paper were collected from unconventional fractured carbonate and tight sandstone reservoirs of Ordovician and Silurian age. However, three gas samples were collected from thermogenic shale gas producing zones in the Ordovician Utica and Point Pleasant shale source rocks.

Reservoirs in the Middle Ordovician Trenton and Black River carbonates (Fig. 2) produce petroleum from dolomitized zones in marine limestones. The dolomitized zones occur around strike-slip faults visible on seismic data that appear controlled by basement structure. The dolomitized zones contain hydrothermal matrix and saddle dolomite formed from hot (100–160 °C), saline (13–17 wt% salinity) Fe and Mn rich brines that migrated through fractures associated with these faults (Patchen et al., 2006). The Upper Ordovician Bald Eagle Sandstone (Fig. 2) produces natural gas from vertical to subvertical fracture sets developed parallel to fold axes on the Appalachian Plateau adjacent to the Allegheny Front. Matrix porosity and permeability averages 5% and 0.07 mD, respectively, but fracture porosity averages 7.8% and can be as high as 30% (Laughrey and Harper, 1996).

Reservoirs in the Lower Silurian Medina Group sandstones comprise a regional petroleum accumulation covering 117,000 km^2 of the Appalachian Basin foreland. The eastern gas bearing portion of the regional Medina play is a basin center gas accumulation. In contrast, the western part contains conventional oil and gas accumulations with hybrid features of basin center accumulations (Ryder and Zagorski, 2003). The stratigraphically equivalent Tuscarora Sandstone increases the area of this regional accumulation by another 78,000 km^2. The sandstones were deposited as part of the clastic wedge that formed during the terminal phase of the Taconic orogeny. Thickness of the clastic wedge ranges from 172 to 183 m in central Pennsylvania and northern West Virginia depocenters to about 30 m or less in southern and central Ohio, northern New York, and southern Ontario in Canada. These sandstones are tight gas reservoirs with average porosity of 7.8% and low permeability (<0.1 mD) in which most of the porosity is secondary due to diagenetic leaching.

2.1.2. Thermal and burial history

New data on thermal maturation of lower Palaeozoic sediments in the Appalachian Basin (Repetski et al., 2008) shows that the most deeply buried reservoir and source rocks for gases in this study reached conodont alteration indices (CAI) >5. Although lower Paleozoic sediments do not contain vitrinite, correlations between many different indexes of thermal maturation indicate that CAI = 5

approximates a vitrinite R_o = 5%. Modeling of the thermal history of the northern Appalachian Basin (Rowan, 2006; Repetski et al., 2008) shows that at maximum burial during the Alleghenian orogeny Silurian and Ordovician age sediments reached temperatures on the order of 250–300 °C. These temperatures are supported by evidence for mineral reactions such as formation of pyrophyllite from kaolinite and quartz (Harrison et al., 2004, and references therein) and fluid inclusion studies (Kisch and van den Kerkhof, 1991; Cook et al., 2006; O'Kane et al., 2007; Onasch et al., 2009). Such temperatures are generally assumed to be the maximum temperature for preservation of low molecular weight hydrocarbons in sedimentary rocks (Hunt, 1996).

2.2. Sample collection and analysis

We collected and analyzed 61 new samples of gas from reservoirs of Silurian and Ordovician age in Ohio, Pennsylvania, New York, West Virginia and Kentucky. The geographic distribution and stratigraphic setting of the reservoirs is shown in Figs. 1 and 2, respectively. The gases were collected from reservoirs that range in depth from 1.5–4.0 km. At depths <1.9 km they produce hydrocarbon liquids (oil and condensate) as well as gas. We classify these gases as oil associated gases (OAG). Reservoirs at greater depth do not produce hydrocarbon liquids and the gases are classified as non-associated gases (NAG).

All samples were collected at the wellhead in stainless steel vessels at wellhead pressure, or through a pressure regulator in aluminium Isotubes® at lower pressure. Analyses were performed at Isotech Laboratories, Inc. using standard analytical protocols. Individual hydrocarbons were separated by cryogenic techniques or on-line gas chromatography. Isotopic compositions are reported relative to Peedee belemnite (VPDB) standard for carbon and relative to standard mean ocean water (SMOW) for hydrogen. Precisions for individual components in the molecular analysis are ±2% and ±0.1‰ for $\delta^{13}C$ by cryogenic separation and ±0.3‰ for $\delta^{13}C$ by on-line continuous flow gas chromatography–isotope ratio–mass spectrometry. Precisions for $\delta^{2}H$ measurements are ±2‰ by off-line cryogenic separation and ±5‰ by on-line continuous flow methods. The figures show error bars for uncertainty in $\delta^{2}H$ measurements. The uncertainty in $\delta^{13}C$ is less than or equal to the symbol size in the figures. Molecular and isotopic compositions of the gases are given in Table 1. In addition, where appropriate, we have used data from gas reservoirs of equivalent age from the central Appalachian Basin to compare with our results (Dennen et al., 2007).

3. Results

3.1. Hydrocarbons

Standard displays of the isotopic composition of methane are shown in Figs. 3 and 4. The Bernard plot (Bernard et al., 1976) in Fig. 3 shows that the carbon isotopic composition of methane becomes progressively enriched in ^{13}C as the methane content increases from the OAG to the NAG, although the NAG in Ordovician age reservoirs shows wide scatter in isotopic composition. The Schoell plot (Schoell, 1983) of $\delta^{13}C$ versus $\delta^{2}H$ of methane in Fig. 4 shows two distinctly different trends in the measurements. The points along the line labeled "maturation trend" include measurements on all the OAG and the NAG in reservoirs shallower than 2600 m. Along this trend both ^{13}C and ^{2}H and become isotopically heavier with increasing methane content, typical for increasing levels of thermal maturation. This trend is similar to the trend of methane compositions from experimental cracking of middle Ordovician age organic matter at progressively higher temperatures (Berner et al., 1995). Furthermore, the trend extrapolates to the range of isotopic compositions measured on organic matter from middle Ordovician age source rocks (Mastalerz et al., 2003, discussed further below). In the second trend, methane in the deepest samples of NAG in Ordovician age reservoirs becomes progressively depleted in ^{2}H as the methane becomes enriched in ^{13}C. The variation of $\delta^{2}H$ in methane with depth is shown in Fig. 5.

Compound specific $\delta^{13}C$ of C_1 to C_4 displayed in natural gas plots (Chung et al., 1988) shown in Fig. 6 show distinct differences between OAG and NAG. The OAG compositions, (Fig. 6A) approximate the linear trends predicted for gases generated by Rayleigh-type fractionation with the model described by Chung (Chung et al., 1988; Rooney et al., 1995). The trends for C_2 to C_4 extrapolate to a possible source composition that is consistent with the most isotopically enriched end member of the two types of organic matter observed in source rocks of middle Ordovician age (Hatch et al., 1987; Mastalerz et al., 2003). The slopes of the trends are also consistent with theoretical kinetic isotope effects (KIEs) calculated with an *ab initio* model of isotope fractionation at temperatures between 127 °C and 227 °C (Tang et al., 2000). The deviation of methane from the normal trend may be due to addition of a small amount of more thermally mature methane. The natural gas plot of the NAG (Fig. 6B) shows reversal of the normal $\delta^{13}C$ trend for C_1, C_2 and C_3 in all samples. The shallowest sample of NAG in a Silurian age reservoir contained enough C_4 for isotopic analysis and shows a return to the normal trend for $\delta^{13}C_3$ and $\delta^{13}C_4$. The slope of trend for $\delta^{13}C_3$ and $\delta^{13}C_4$ is consistent with the *ab initio* model of fractionation between 127 °C and 227 °C if the $\delta^{13}C$ of the source is the depleted end member of the range for middle Ordovician age *G. Prisca* rich organic matter.

To provide additional information to constrain the origin of the reversals in the carbon isotopic compositions we analyzed the ^{2}H compositions of the C_2 + gases. Only a subset of the samples was available for additional analysis. All measurements are listed in Table 1 and representative measurements for individual accumulations are shown in Fig. 7. The OAG show enrichment in ^{13}C and ^{2}H with increasing carbon number as observed in OAG in other parts of the Appalachian basin (Barker and Pollock, 1984; Sherwood Lollar et al., 2002; Dennen et al., 2007) and other sedimentary basins (Prinzhofer and Huc, 1995; Hulston et al., 2001). The NAG did not contain enough C_3 and higher hydrocarbons to allow analysis of ^{2}H. For most samples with $\delta^{13}C$ reversed between C_1 and C_2, $\delta^{2}H$ is also reversed.

3.2. Non-hydrocarbons

All gas samples contain measurable amounts of N_2 with three samples containing more than 10 mol%. $\delta^{15}N$ was measured on a large fraction of the samples. The CO_2 content ranges from below detection limit to about 1.2 mol% and $\delta^{13}C$ was measured on a small number of samples. Only one sample contained detectable H_2S with $\delta^{34}S$ = +14.7‰. Relationships between N_2 content, $\delta^{15}N$, CO_2 content, $\delta^{13}C$, including the relationship between $\delta^{13}C$ CO_2 and $\delta^{13}C$ CH_4 are shown in Fig. 8.

4. Discussion

4.1. Stable isotopic and molecular compositions

4.1.1. Correlation of gases to source organic matter

Measurements of the $\delta^{13}C$ and $\delta^{2}H$ of organic matter in sedimentary rocks of middle Ordovician age from well characterized localities in North America and Europe (Hatch et al., 1987; Mastalerz et al., 2003) show an 8‰ range in $\delta^{13}C$ as a function of sedimentary facies but relatively little variation in ^{2}H. If we display

Table 1
Molecular and compound specific stable isotopic compositions of gases. Field types OAG and NAG are oil associated gases and non-associated gases, respectively. The US state abbreviations are Kentucky (KY), New York (NY), Ohio (OH), Pennsylvania (PA), and West Virginia (WV).

Field type	State	Field name	Reservoir age	Well name	Producing reservoir	Mean Pert. depth (m)	CH_4 (mol%)	C_2 (mol%)	C_3 (mol%)	*i*-C_4 (mol%)	*n*-C_4 (mol%)	*i*-C_5 (mol%)	*n*-C_5 (mol%)	C_6+ (mol%)	N_2 (mol%)	O_2 (mol%)	Co_2 (mol%)	H_2S (mol%)	$\delta^{13}C$ CH_4 (‰)	$\delta^{2}H$ CH_4 (‰)	$\delta^{13}C_2$ (‰)	$\delta^{2}H$ C_2 (‰)	$\delta^{13}C_3$ (‰)	$\delta^{2}H$ C_3 (‰)	$\delta^{13}C$ *i*-C_4 (‰)	$\delta^{13}C$ *n*-C_4 (‰)	$\delta^{13}C$ *n*-C_5 (‰)	$\delta^{13}CO_2$ (‰)	$\delta^{15}N$ (‰)	$\delta^{34}S$ (‰)
NAG	PA	MARSHLANDS	Silurian	MLU#1	Tuscarora	2926.5	94.37	2.220	0.1800	0.0155	0.0213	0.0065	0.0021	0.0053	2.96	0.0217	0.091	0.00	−27.79	−159.7	−36.76	−191.7	−39.70	–	–	–	–	–	−11.40	
NAG	PA	MARSHLANDS	Silurian	MLU#3	Tuscarora	2861.5	94.38	2.200	0.1790	0.0154	0.0217	0.0067	0.0019	0.0053	2.94	0.0211	0.120	0.00	−27.68	−158.4	−36.66	−191.2	−39.50	–	–	–	–	–	−10.90	–
NAG	PA	DEVIL'S ELBOW	Silurian	Shaw#1	Tuscarora	3583.3	96.2	2.300	0.2000	0.0000	0.0000	0.0000	0.0000	0.2000	1.10	0.0000	0.200	0.00	−37.40	−150	–	–	–	–	–	–	–	–	–	–
NAG	PA	DEVIL'S ELBOW	Silurian	C and K Coal #1	Tuscarora	3637.1	80.68	2.750	0.2000	0.0190	0.0240	0.0092	0.0020	0.0075	16.19	–	0.090	–	−32.72	−164.6	−40.04	–	−41.49	–	–	–	–	–	–	–
NAG	PA	–	Silurian	Spring Creek	Medina	–	91.8	4.200	0.8000	–	–	–	–	0.6000	2.70	–	–	–	−36.80	−163.4	−36.28	–	−31.59	–	–	–	–	–	–	–
NAG	PA	–	Silurian	Ellen 3	Medina	1802.5	94.2	2.500	0.2000	–	–	–	–	0.4000	2.90	–	–	–	−34.40	−154.2	−39.57	–	−38.21	–	–	–	–	–	–	–
NAG	PA	–	Silurian	Dailey 1	Medina	1735.8	93.1	3.300	0.5000	–	–	–	–	0.4000	2.80	–	–	–	−35.50	−157	−36.53	–	−31.01	–	–	–	–	–	–	–
NAG	NY	GLODES CORNERS	Ordovician	Radigan	Black River	2195.4	97.74	0.683	0.0194	0.0000	0.0000	0.0000	0.0000	0.0000	1.42	0.0000	0.079	0.00	−31.94	−148.7	−39.17	−168.9	–	–	–	–	–	−2.40	–
NAG	NY	GLODES CORNERS	Ordovician	Levandowski	Black River	2368.1	96.89	0.677	0.0210	0.0000	0.0000	0.0000	0.0000	0.0000	2.14	0.0000	0.000	0.00	−32.45	−146.5	−39.64	−169.9	–	–	–	–	–	−2.40	–
NAG	NY	GLODES CORNERS	Ordovician	Fox	Black River	2311.0	97.30	0.665	0.0215	0.0000	0.0000	0.0000	0.0000	0.0000	1.85	0.0000	0.091	0.00	−32.38	−145.5	−39.61	−168.6	–	–	–	–	–	−2.40	–
NAG	NY	GLODES CORNERS	Ordovician	Gray	Black River	2422.4	96.67	0.383	0.0065	0.0000	0.0000	0.0000	0.0000	0.0000	2.41	0.0000	0.000	0.00	−32.77	−146.6	−39.65	−167.3	–	–	–	–	–	−2.40	–
NAG	NY	GLODES CORNERS	Ordovician	Covert #1	Black River	2367.1	94.97	0.600	0.0171	0.0000	0.0000	0.0000	0.0000	0.0000	2.11	0.0000	0.000	0.00	−32.48	−145.1	−39.73	−168.2	–	–	–	–	–	−2.40	–
NAG	NY	MUCK FARM	Ordovician	McAllister	Black River	2342.4	97.81	0.815	0.0309	0.0012	0.0019	0.0000	0.0000	0.0314	1.18	0.0000	0.070	0.00	−31.53	−148.2	−38.95	−171.5	–	–	–	–	–	−3.10	–
NAG	NY	COUNTY LINE	Ordovician	Purvis #1	Black River	2989.0	98.46	0.675	0.0232	0.0000	0.0013	0.0000	0.0000	0.0000	0.65	0.0000	0.160	0.00	−29.94	−150.4	−37.63	−140.2	–	–	–	–	–	−3.90	–
NAG	NY	ZIMMERHILL	Ordovician	Drumm#1	Black River	3433.1	98.82	0.646	0.0242	0.0000	0.0019	0.0000	0.0000	0.0000	0.39	0.0000	0.100	0.00	−31.63	−151.1	−38.81	−169.6	−39.80	–	–	–	–	−6.6	−10.21	
NAG	NY	TERRY HILL SOUTH	Ordovician	Kimbell	Black River	2984.9	98.54	0.661	0.0234	0.0000	0.0015	0.0000	0.0000	0.0177	0.54	0.0000	0.190	0.00	−29.83	−149.5	−37.52	−154	–	–	–	–	–	−3.10	–
NAG	NY	TERRY HILL SOUTH	Ordovician	Lant#1	Black River	2957.3	98.53	0.709	0.0260	0.0000	0.0016	0.0000	0.0000	0.0000	0.52	0.0000	0.180	0.00	−30.09	−150.9	−37.61	−157.4	−39.18	–	–	–	–	−5.8	−7.68	
NAG	NY	WILSON HOLLOW	Ordovician	Jimerson #1	Black River	3168.6	98.51	0.721	0.0271	0.0000	0.0018	0.0000	0.0000	0.0000	0.54	0.0000	0.170	0.00	−30.10	−149.2	−37.96	−165.5	–	–	–	–	–	−4.20	–
NAG	NY	QUACKENBUSH	Ordovician	Gregory	Black River	3095.8	98.96	0.518	0.0183	0.0000	0.0000	0.0000	0.0000	0.0000	0.24	0.0000	0.250	0.00	−29.09	−150.6		–	–	–	–	–	–	–	–	–
NAG	NY	QUACKENBUSH	Ordovician	Soderblom	Black River	3470.5	99.14	0.362	0.0129	0.0000	0.0000	0.0000	0.0000	0.0000	0.10	0.0000	0.370	0.00	−29.23	−148.6	–	–	–	–	–	–	–	–	–	–
NAG	NY	QUACKENBUSH	Ordovician	Lovell	Black River	3200.6	98.65	0.571	0.0202	0.0000	0.0013	0.0000	0.0000	0.0000	0.48	0.0056	0.250	0.00	−29.65	−152.6	−36.97	−146.9	−38.52	–	–	–	–	−5.6	−7.57	
NAG	NY	QUACKENBUSH	Ordovician	Hakes #1	Black River	3647.6	98.71	0.547	0.0194	0.0000	0.0010	0.0000	0.0000	0.0000	0.48	0.0065	0.210	0.00	−29.94	−152.1	−37.15	−145.4	−39.13	–	–	–	–	−5.7	−7.81	–
NAG	NY	QUACKENBUSH	Ordovician	#1 Andrews	Black River	3715.7	98.63	0.610	0.0218	0.0000	0.0013	0.0000	0.0000	0.0000	0.46	0.0000	0.250		−29.56	−151.2	−37.07	–	–	–	–	–	–	–	–	–
NAG	NY	LANGDON HILL	Ordovician	Konstantinides #1	Black River	3355.3	97.47	0.640	0.0207	0.0000	0.0000	0.0000	0.0000	0.0000	1.63	0.0197	0.150	0.00	−26.02	−155.1	−33.04	−155.6	−34.51	–	–	–	–	−5.2	−2.59	–
NAG	NY	RAYNER	Ordovician	Gillis#1	Black River	3646.5	98.58	0.617	0.0221	0.0000	0.0016	0.0000	0.0000	0.0000	0.46	0.0000	0.300	0.00	−27.85	−152.9	−34.67	−138.5	−36.56	–	–	–	–	−6.7	−7.61	–
NAG	NY	LAUREL RUN	Ordovician	Harvey	Black River	3640.9	98.59	0.586	0.0203	0.0000	0.0014	0.0000	0.0000	0.0000	0.47	0.0000	0.310	0.00	−27.48	−154.4	−34.28	−148.2	−35.94	–	–	–	–	−4.7	−8.17	–
NAG	NY	SEELEY CREEK	Ordovician	Curren #1	Black River	3693.7	98.98	0.398	0.0148	0.0000	0.0000	0.0000	0.0000	0.0000	0.31	0.0000	0.270	0.00	−26.24	−155.3	−32.71	−137.1	−33.87	–	–	–	–	−5.0	−8.93	–
NAG	PA	STAGECOACH	Ordovician	Koder#1	Black River	4150.3	92.32	0.925	0.0555	0.0058	0.0254	0.0105	0.0146	0.0251	6.06	0.0094	0.460	0.00	−27.25	−154.6	−34.59	–	–	–	–	–	–	–	–	–
NAG	PA	Wildcat well	Ordovician	Wolpert#1	Black River	3508.9	84.42	0.552	0.0184	0.0000	0.0000	0.0000	0.0000	0.0270	14.14	0.0000	0.140	0.51	−26.54	−156.6	−31.5		−28.30	–	–	–	–	−3.0	0.40	14.7
NAG	PA	Wildcat well	Ordovician	Starvaggi #1	Black River	3508.9	97.81	0.820	0.0389	0.0026	0.0036	0.0000	0.0000	0.0000	1.01	0.0063	0.260	0.00	−34.85	−148.1	−39.95	–	−38.73	–	–	–	–	−3.2	−1.92	–
NAG	PA	MARSHLANDS	Ordovician	MLU#2	Point Pleasant	3933.7	97.15	1.260	0.0785	0.0000	0.0047	0.0000	0.0000	0.0000	–	–	–	–	–	–	–	–	–	–	–	–	–	–		–
NAG	PA	MARSHLANDS	Ordovician	MLU#2	Utica	3864.8	96.88	1.220	0.0734	0.0000	0.0045	0.0000	0.0000	0.0000	0.66	0.0453	1.080	0.00	−26.97	−156	−34.68	−173.7	−37.00	–	–	–	–	−0.4	−9.20	–
NAG	PA	GRUGAN	Ordovician	PA State Tr. 289	Bald Eagle	4320.5	95.9	2.000	0.2000	0.0000	0.0000	0.0000	0.0000	0.0000	1.50	0.0000	0.200	0.00	−27.20	−154.9	−35.83	–	−37.41	–	–	–	–	–	–	–
NAG	WV	COTTONTREE	Ordovician	Parker	Trenton	3367.1	98.98	0.692	0.0417	0.0022	0.0038	0.0000	0.0000	0.0176	0.14	0.0000	0.110	0.00	−35.43	−133.8	−38.26	–	–	–	–	–	–	–	–	–
NAG	WV	COTTONTREE	Ordovician	Epling	Trenton	–	98.71	0.875	0.0655	0.0022	0.0031	0.0000	0.0000	0.0000	0.16	0.0000	0.170	0.00	−35.12	−133.1	−37.47	–	–	–	–	–	–	–	–	–
OAG	OH	YORK	Ordovician	Downes #1	Black River	1665.5	90.68	4.650	1.7000	0.2870	0.5750	0.1730	0.1710	0.2770	1.38	0.0088	0.009	0.00	−37.38	−165.4	−34.37	−161.1	−30.44	−128.1	−30.26	−29.25	−28.6	–	−0.90	–
OAG	OH	YORK	Ordovician	Downes #3	Black River	1625.8	90.47	4.690	1.7500	0.3000	0.6170	0.1910	0.1970	0.3630	1.33	0.0000	0.027	0.00	−37.37	−166.9	−34.38	−159	−30.50	−129.4	−30.30	−29.21	−28.61	–	−0.90	
OAG	OH	YORK	Ordovician	Riffle #1	Black River	1667.8	90.44	5.040	1.6800	0.2620	0.5650	0.1570	0.1610	0.3610	1.25	0.0000	0.023	0.00	−37.41	−166.8	−34.36	−159.8	−30.48	−133.9	−30.32	−29.36	−28.75	–	−4.00	–
OAG	OH	YORK	Ordovician	Dalin #1	Black River	1623.5	89.77	4.920	1.9200	0.3400	0.7290	0.2500	0.2590	0.3680	1.34	0.0000	0.044	0.00	−37.50	−167.3	−34.48	−157.1	−30.59	−130.3	−30.31	−29.33	−28.54	–	−1.50	
OAG	OH	YORK	Ordovician	York#1	Black River	1680.9	89.42	4.740	1.8000	0.3170	0.6720	0.2260	0.2480	0.8030	1.63	0.0302	0.046	0.00	−37.44	−168.5	−34.44	−157.9	−30.50	−133.6	−30.31	−29.34	−28.54	–	−1.20	–
OAG	OH	YORK	Ordovician	Mantell #1	Black River	1713.7	90.00	4.450	1.7000	0.3050	0.6500	0.2410	0.2720	0.5020	1.61	0.0000	0.000	0.00	−38.04	−168.9	−34.75	−159.8	−30.83	−134.5	−30.40	−29.45	−28.7	–	−1.30	
OAG	KY	HOMER	Ordovician	Wheeler 24	Trenton	–	91.38	4.140	1.4900	0.1830	0.3470	0.0499	0.0418	0.0354	2.23	0.0000	0.000	0.00	−39.50	−143.4	−36.83	–	−31.36	–	−30.95	−29.93	–	–	–	–
OAG	KY	HOMER	Ordovician	Oliver 50 (T2)	Trenton	–	88.03	5.460	2.2900	0.3410	0.7550	0.1900	0.2170	0.1880	2.35	0.0063	0.081	0.00	−40.30	−147.6	−36.67	–	−31.45	–	−31.59	−30.22	–	–	–	–
OAG	KY	HOMER	Ordovician	Lawson Heirs (T1)	Trenton	–	81.64	7.810	3.5400	0.3500	0.9200	0.1700	0.2000	0.2300	4.75	nd	0.060	0.00	−44.41	−206.9	−37.71	–	−33.92	–	–	−31.57	−30.46	–	–	–
OAG	KY	COLIN FORK	Ordovician	Milton	Trenton		86.89	4.720	1.6500	0.3320	0.5460	0.1420	0.1440	0.1620	5.17	0.0065	0.011	0.00	−44.76	−166.3	–	–	–	–	–	–	–	–	–	–
OAG	OH	LSRA	Silurian	Patterson #2 well	Clinton/ Medina	1180.9	78.03	9.700	4.8200	0.6000	1.3300	0.3000	0.3000	0.2200	4.55	0.0000	0.000	–	−41.98	−201.9	−35.26	–	−32.34	–	–	−30.68	–	–	−4.92	–
OAG	OH	LSRA	Silurian	Bruno #1 well	Clinton/	1253.1	85.62	6.180	2.5600	0.3600	0.7300	0.1900	0.1700	0.1600	3.91	0.0000	0.000	–	−39.17	−174.1	−33.76	–	−31.10	–	–	–	–	–		

(*continued on next page*)

Table 1 (*continued*)

Field type	State	Field name	Reservoir age	Well name	Producing reservoir	Mean Pert. depth (m)	CH_4 (mol%)	C_2 (mol%)	C_3 (mol%)	*i*-C_4 (mol%)	*n*-C_4 (mol%)	*i*-C_5 (mol%)	*n*-C_5 (mol%)	C_6+ (mol%)	N_2 (mol%)	O_2 (mol%)	Co_2 (mol%)	H_2S (mol%)	$\delta^{13}C$ CH_4 (‰)	δ^2H CH_4 (‰)	$\delta^{13}C_2$ (‰)	δ^2H C_2 (‰)	$\delta^{13}C_3$ (‰)	δ^2H C_3 (‰)	$\delta^{13}C$ *i*-C_4 (‰)	$\delta^{13}C$ *n*-C_4 (‰)	$\delta^{13}C$ *n*-C_5 (‰)	$\delta^{13}CO_2$ (‰)	$\delta^{15}N$ (‰)	$\delta^{34}S$ (‰)
OAG	OH	LSRA	Silurian	Grandview – Johnson #2	Medina Clinton/ Medina	1290.7	88.10	5.300	2.1600	0.3600	0.7200	0.2100	0.1800	0.2300	2.63	0.0000	0.000	–	–38.06	–167.3	–34.62	–	–30.81	–	–	–29.52	–	–	–2.98	–
OAG	OH	LSRA	Silurian	Hissa #2 well	Clinton/ Medina	1299.5	76.38	10.980	6.0700	1.0600	2.0100	0.6000	0.5200	0.2800	2.01	0.0000	0.020	–	–39.83	–181.9	–35.16	–	–31.18	–	–	–	–	–	–	–
OAG	OH	LSRA	Silurian	Detweiler#1 well	Clinton/ Medina	1262.1	88.17	5.580	1.9300	0.2800	0.5100	0.1400	0.1200	0.1100	3.04	0.0000	0.020	–	–38.76	–174.3	–35.12	–	–30.90	–	–	–	–	–	–	–
OAG	OH	LSRA	Silurian	D. French #2 well	Clinton/ Medina	1246.9	87.48	5.590	2.1200	0.3300	0.6300	0.1700	0.1500	0.1400	3.24	0.0000	0.020	–	–38.78	–174.6	–35.26	–	–31.05	–	–	–	–	–	–	–
OAG	OH	LSRA	Silurian	H. Griffin #3 well	Clinton/ Medina	1249.3	88.19	5.170	1.8700	0.2600	0.5100	0.1300	0.1200	0.0980	3.54	0.0000	0.000	–	–38.75	–175.3	–35.58	–	–31.34	–	–	–29.84	–	–	–1.31	–
OAG	OH	LSRA	Silurian	Clemens #2	Clinton/ Medina	1405.8	90.64	4.480	1.3200	0.1800	0.3100	0.0850	0.0960	0.1200	2.67	0.0000	0.000	–	–37.40	–165.7	–34.67	–	–30.40	–	–	–	–	–	–	–
OAG	OH	LSRA	Silurian	Krantz #2	Clinton/ Medina	1435.9	89.34	5.110	1.6500	0.2200	0.4000	0.1100	0.1100	0.1200	2.84	0.0000	0.010	–	–37.49	–168.5	–35.29	–	–30.94	–	–	–	–	–	–	–
OAG	OH	LSRA	Silurian	#1 Governor	Clinton/ Medina	1444.2	90.33	4.640	1.4700	0.2000	0.3800	0.1100	0.1300	0.1400	2.50	0.0000	0.010	–	–37.20	–166.6	–34.88	–	–30.58	–	–	–	–	–	–	–
OAG	PA	LSRA	Silurian	Oris #8 well	Clinton/ Medina	1595.6	89.94	4.580	1.3500	0.2200	0.3600	0.1100	0.0890	0.1600	3.08	0.0000	0.010	–	–36.90	–167.3	–35.32	–	–30.61	–	–	–	–	–	–	–
OAG	PA	LSRA	Silurian	Gibson #2 well	Clinton/ Medina	1637.0	91.74	3.670	0.8700	0.1300	0.2500	0.0780	0.0610	0.0870	2.99	0.0000	0.020	–	–35.58	–159.8	–35.98	–	–30.74	–	–	–29.24	–	–	–5.00	–
NAG	PA	LSRA	Silurian	Brown #5 well	Clinton/ Medina	2085.6	94.36	2.370	0.1500	0.0170	0.0220	0.0090	0.0000	0.0150	2.92	0.0000	0.040	–	–34.69	–152.3	–39.75	–	–40.17	–	–	–	–	–	–	–
NAG	PA	LSRA	Silurian	Velasaris #1 well	Clinton/ Medina	2151.2	94.25	2.260	0.1400	0.0150	0.0170	0.0073	0.0000	0.0090	3.17	0.0000	0.040	–	–34.19	–153.3	–41.14	–	–42.85	–	–	–38.89	–	–	–5.14	–
NAG	PA	LSRA	Silurian	#2 Mathews well	Clinton/ Medina	2155.2	94.02	2.230	0.1300	0.0140	0.0170	0.0070	0.0016	0.0087	3.45	0.0000	0.030	–	–33.97	–150.8	–41.15	–	–42.81	–	–	–	–	–	–	–

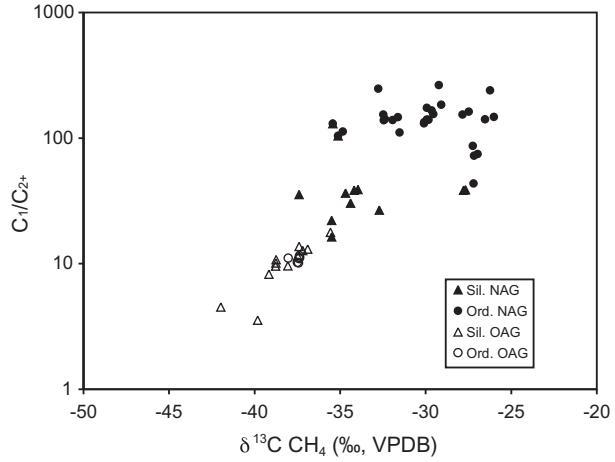

Fig. 3. Bernard plot of $\delta^{13}C_1$ versus C_1/C_2+ (Bernard et al., 1976). The gases show a general trend of enrichment in ^{13}C as gases become richer in methane, with a clear trend for OAG but wide scatter for the NAG. Note that symbols for OAG and NAG samples from Ordovician and Silurian age reservoirs are used in all subsequent figures.

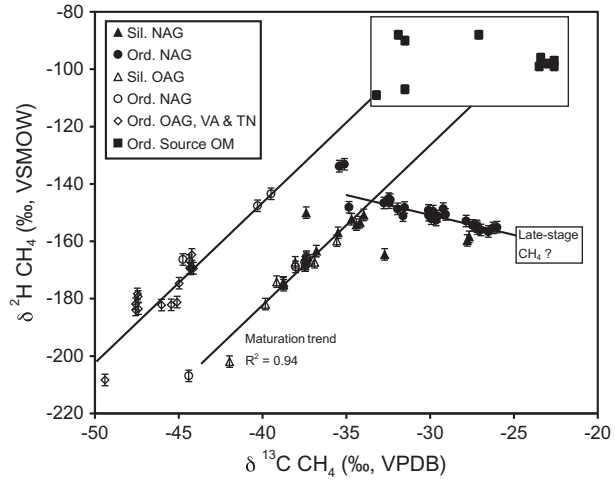

Fig. 4. Schoell plot of $\delta^{13}C$ versus δ^2H for methane in OAG, NAG, and middle Ordovician organic matter. Compositions fall on two distinct trends. Trend 1 (R^2 = 0.94), labeled "maturation trend" extends through the OAG and Silurian NAG showing progressive enrichment in ^{13}C and ^2H, typical of a maturation sequence (Schoell, 1983). This trend extrapolates to the isotopically enriched compositions of middle Ordovician age organic matter (Hatch et al., 1987; Mastalerz et al., 2003). Additional data for OAG from reservoirs in Virginia (VA) and Tennessee (TN) (Dennen et al., 2007) fall on a parallel line that extends to the isotopically depleted compositions of possible middle Ordovician sources. The OAG from VA and TN are associated with oils with characteristics consistent with generation from *G. prisca*-rich organic matter (Dennen et al., 2007). The second trend (R^2 = 0.80) extends through the measurements in the Ordovician NAG in the deepest reservoirs and shows distinct depletion in ^2H as methane becomes progressively more enriched in ^{13}C. The extension of this trend to the box labeled "late-stage CH_4" is discussed in the text.

these measurements on a Schoell plot (Fig. 4) with our measurements on methane and include OAG from Ordovician age reservoirs in the central Appalachians (Dennen et al., 2007), the gas measurements fall on two parallel trends that extrapolate to the measurements on source organic matter. Furthermore, the hydrocarbon liquids produced with gases on the two parallel isotopic trends are also consistent with sources that contain the two end members of middle Ordovician age organic matter. The liquids most depleted in ^{13}C show odd carbon predominance in the *n*-alkanes typical for liquids generated from *G. prisca*-rich organic

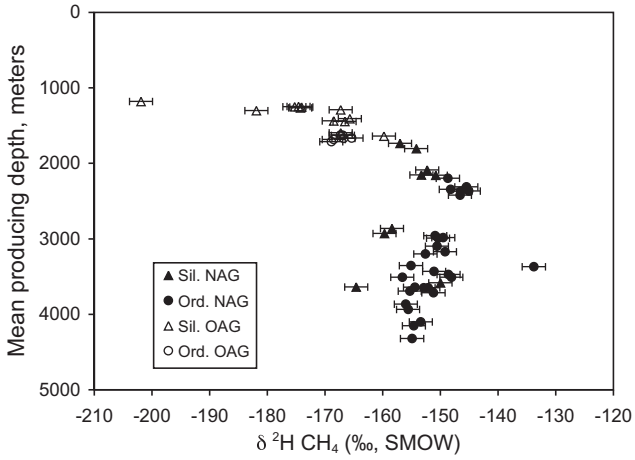

Fig. 5. δ^2H of methane versus mean production depth. Below 2500 m NAG show a reversal in the commonly observed trend of increasing isotopic enrichment with depth. One deep NAG sample, Cottontree, WV, deviates from this reversed trend.

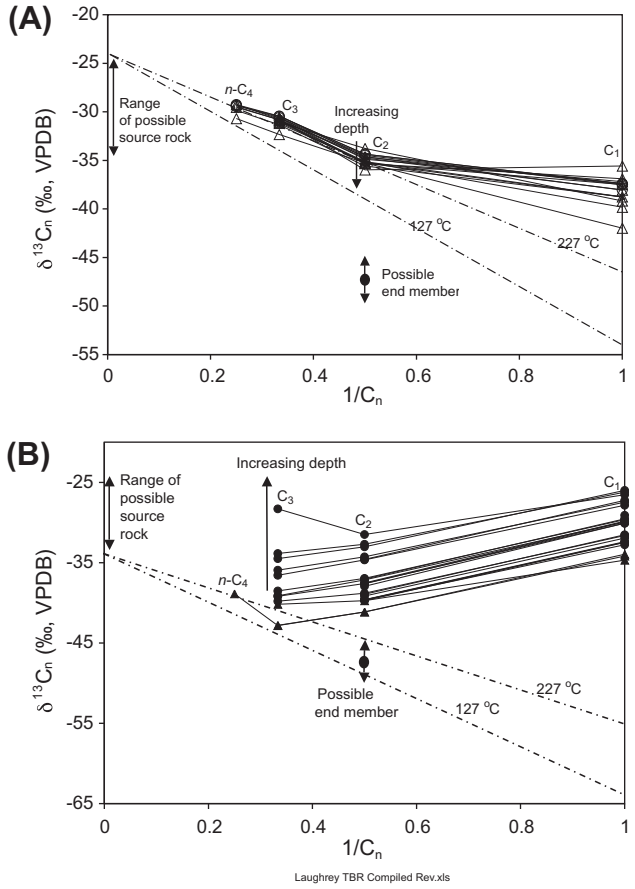

Fig. 6. Natural gas plots (Chung et al., 1988) for OAG and NAG. (A) $\delta^{13}C$ variations in OAG along with the theoretical trends for gases cracked at 127 and 227 °C from alkanes generated at the ^{13}C enriched end of the range for source rocks of middle Ordovician age. The gases are not isotopically reversed and the measurements for C_2 to n-C_4 are consistent with the theoretical trends. (B) $\delta^{13}C$ variations in the NAG with the same theoretical trends for cracking from the isotopically depleted end of the range for source rocks of middle Ordovician age. All C_1 to C_3 gases are isotopically reversed. The point labeled "possible endmember" is a hypothetical isotopic composition for ethane generated at temperatures between 127 and 227 °C from isotopically depleted middle Ordovician source rocks.

matter (Dennen et al., 2007) whereas the liquids produced with isotopically heavier gases do not (Burruss and Ryder, 2003) consistent

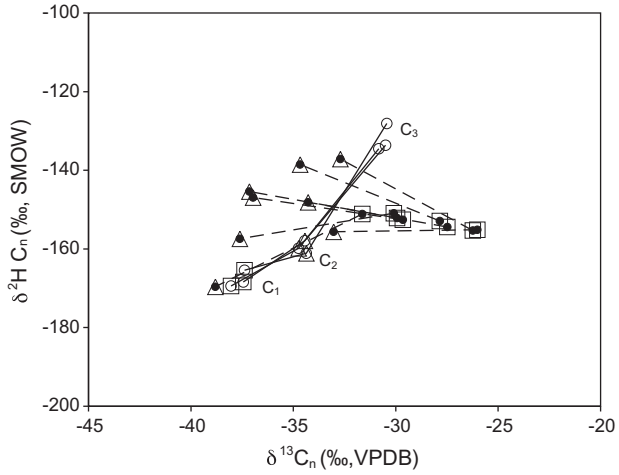

Fig. 7. Compound specific $\delta^{13}C$ versus δ^2H for C_1 to C_3 in Ordovician OAG gases in three samples from the York field, Ohio, and NAG from several fields in New York. The OAG are shown as open symbols connected with solid lines and the measurements follow a normal trend of progressive enrichment in ^{13}C and δ^2H with carbon number. The NAG are shown as solid symbols connected with dashed lines and the isotopic compositions are reversed. The distinction between normal and reversed trends is highlighted by outlining the values for C_1 in squares and C_2 in triangles. Error bars on δ^2H measurements are omitted for clarity.

with the range of compositions of extracts from source rocks of this age (Hatch et al., 1987). These observations establish a strong correlation between the gases and source rocks in the Utica Formation and the stratigraphically equivalent Antes Formation in the northern Appalachian basin.

4.1.2. Identification of mixing and alteration effects

The range of isotopic compositions of middle Ordovician age organic matter suggests that some part of the range of isotopic compositions of gases, including isotopic reversals was caused by mixing of gases. The other possibility, given the maximum temperatures achieved during burial history of the deepest samples, is that hydrocarbons were lost from the system by cracking or oxidative reactions. Loss of significant fractions of the original concentrations of ethane and propane could lead to shifts of isotopic composition to heavier values through Rayleigh-type fractionation. We used standard diagnostic plots of isotopic composition and concentration of individual components (Kendall and Caldwell, 1998) to separate the effects of mixing and Rayleigh fractionation.

Fig. 9 illustrates our process for identifying the effects of mixing and Rayleigh fractionation on ethane (analysis of the measurements on propane is consistent with this approach but the dataset is smaller). Individual components of mixed gases should plot on straight lines as a function of the inverse of concentration (Kendall and Caldwell, 1998). Ethane compositions for the OAG in Ordovician and Silurian age reservoirs and the NAG in Silurian age reservoirs form a linear array (Fig. 9A). The equation for a line fit to these points results in progressive depletion of ethane ^{13}C with decreasing concentration. The NAG in Ordovician reservoirs (Fig. 9A) contain less than 2 mol% ethane and the points scatter randomly with no evidence of mixing trends.

Rayleigh-type fractionation should cause the isotopic composition to be a linear function of the natural logarithm of the concentration. The measurements for ethane in NAG (Fig. 9B) show wide scatter and no single linear trend is obvious. However, if we make models using theoretical fractionation factors (Tang et al., 2000) between 200 °C and 300 °C ($\alpha = 1.022$ and $\alpha = 1.015$, respectively), and starting compositions along the mixing trend (Fig. 9A), then at an ethane concentration of 1.2 mol% and $\delta^{13}C_2 = -48‰$, the

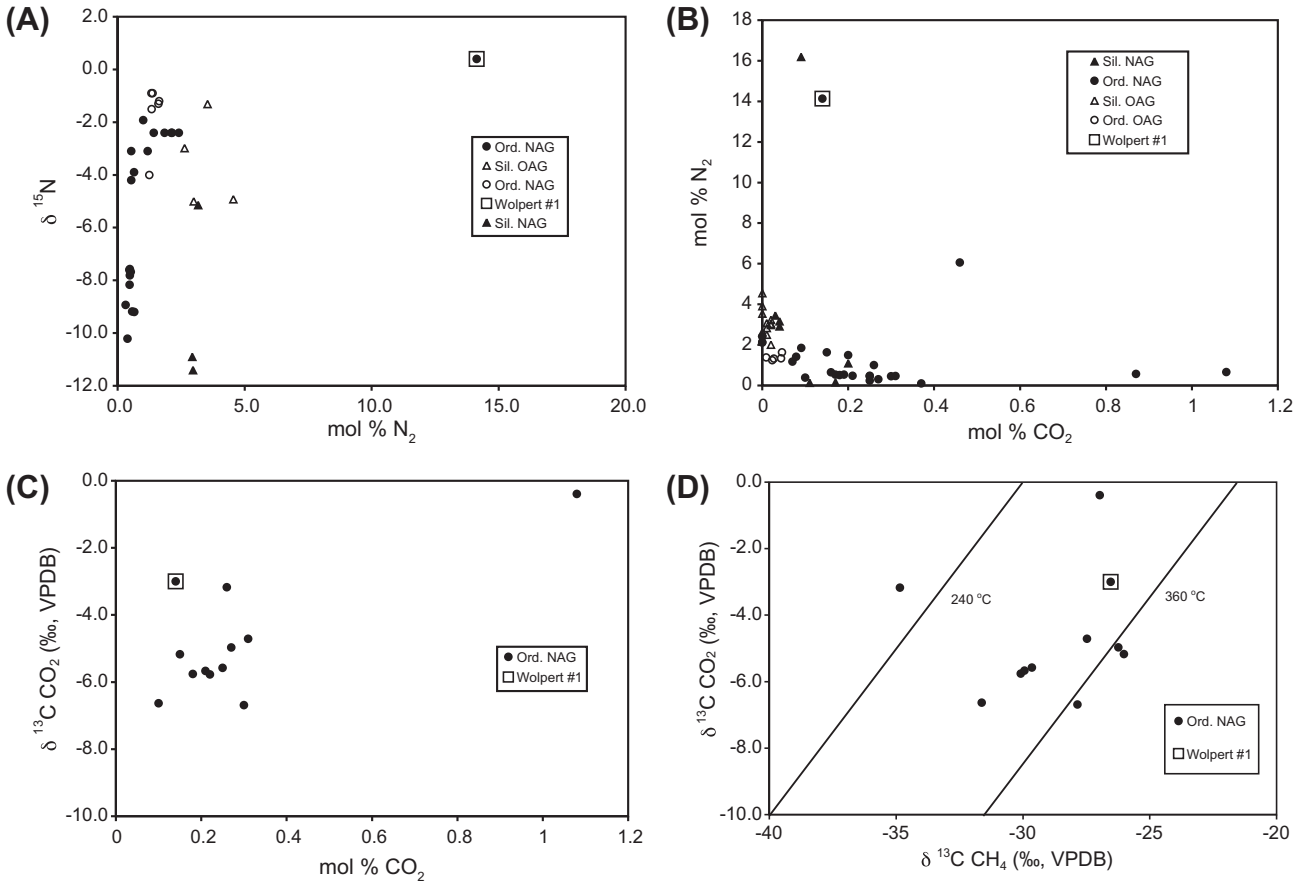

Fig. 8. Molecular and isotopic compositions of non-hydrocarbon gases. The symbol within a box in each panel is the sample from the Wolpert #1 wildcat well, the only sample with detectable H_2S. (A) $\delta^{15}N$ versus nitrogen concentration. (B) The relationship between N_2 and CO_2 concentrations. (C) All measurements of CO_2 concentration and $\delta^{13}C$. Only one sample contains >1 mol% CO_2. (D) $\delta^{13}C$ CO_2 versus $\delta^{13}C$ CH_4. The diagonal lines are ^{13}C fractionation factors calculated for the temperatures indicated (Bottinga, 1969) assuming isotopic equilibrium between CH_4 and CO_2.

Rayleigh-type fractionation trends (Fig. 9B) span the range of most of the measurements on the NAG.

When the mixing and Rayleigh-type fractionation models for ethane (Fig. 9A and B, respectively) are plotted on a linear concentration scale (Fig. 10), reasonable fits to the measurements converge toward an end-member composition of 1.2 mol% C_2 with $\delta^{13}C_2 \sim -48‰$. Although this isotopic composition of ethane is a relatively depleted compared to ethane in most thermogenic natural gases, it is consistent with a model composition for hydrocarbon gases generated from isotopically depleted *G. prisca* rich organic matter. This is indicated by the point labeled "possible end member" in the natural gas plot for the NAG (Fig. 6B).

4.1.3. Methane

The variation of $\delta^{13}C$ with methane concentration in the total gas (Fig. 11) shows a linear array of points that include all the OAG and the NAG in the shallowest reservoirs of Silurian and Ordovician age. Most of the samples in this array (shown with a line to guide the eye) fall along the maturation trend on the Schoell plot that extrapolates to the isotopic compositions for *G. prisca* rich organic matter (Fig. 4) consistent with primary source control on the composition. However, samples from the deepest NAG reservoirs form a more poorly defined array (dashed line) in which $\delta^{13}C$ changes rapidly with increasing C_1 concentration. The apparent change in slope between these two arrays of points is consistent with the reversal in slope on the Schoell plot (Fig. 4) and the change in variation of δ^2H in C_1 with depth (Fig. 5). The methane carbon and hydrogen isotopic compositions and concentration in the NAG from deepest reservoirs do not appear to be consistent with an origin from thermal cracking from primary source organic matter or high molecular weight products from the source. This strongly suggests that other geochemical processes are controlling the isotopic composition of methane in the deepest samples.

4.2. Geochemical processes

4.2.1. Ethane and propane destruction

Although the deepest samples come from production depths of about 4 km, estimates of maximum burial based on thermal maturity (Repetski et al., 2008) are 10–12 km. At geothermal gradients of 20–30 °C/km, maximum source and reservoir temperatures reached about 200–350 °C. At these temperatures, the hydrocarbon reactions can be impacted by the presence of water (Lewan, 1997) and redox active transition metals (Seewald et al., 2006). For example, ethane could be lost by partial reduction with ferrous iron and water (note: In reactions that follow, stoichiometric compositions for magnetite and hematite are shown as proxies for Fe^{2+}/Fe^{3+} or other redox couples in more complex oxyhydroxide and aluminosilicate phases in sedimentary rocks):

$$C_2H_6 + 2Fe_3O_4 + H_2O = 3Fe_2O_3 + 2CH_4 \quad (1)$$

In the absence of transition metal redox couples, ethane can be lost through pyrolysis reactions, such as

$$4C_2H_6 + 2H_2O = 7CH_4 + CO_2 \quad (2)$$

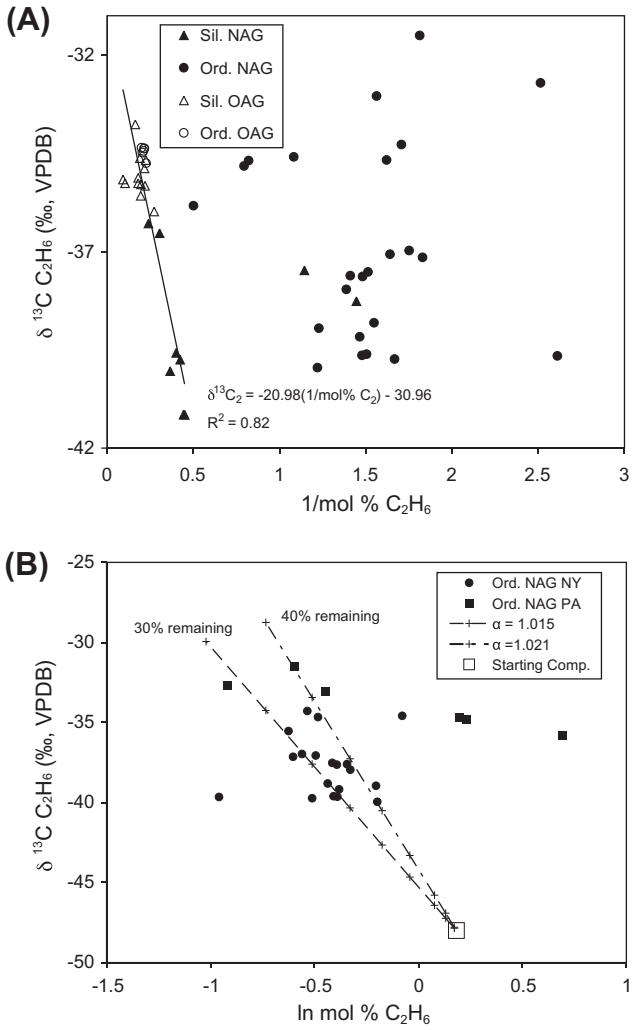

Fig. 9. Evidence for mixing and Rayleigh fractionation effects on ethane. (A) Variations of $\delta^{13}C_2$ with the inverse of concentration in OAG in Silurian and Ordovician reservoirs fall on a linear trend due to mixing, but the NAG in the deeper reservoirs show no obvious mixing relationship. Extrapolation of the equation for the trend results in $\delta^{13}C_2 = -48‰$ at 1.2 mol%. (B): Variations of $\delta^{13}C_2$ with the natural logarithm of the concentration in NAG show that most of the measurements for gases in accumulations in New York state are bounded by a Rayleigh fractionation model with a starting composition (within box) of 1.2 mol% and $\delta^{13}C_2 = -48‰$ and $\alpha = 1.022–1.015$ ($T = 200–300$ °C, (Tang et al., 2000)).

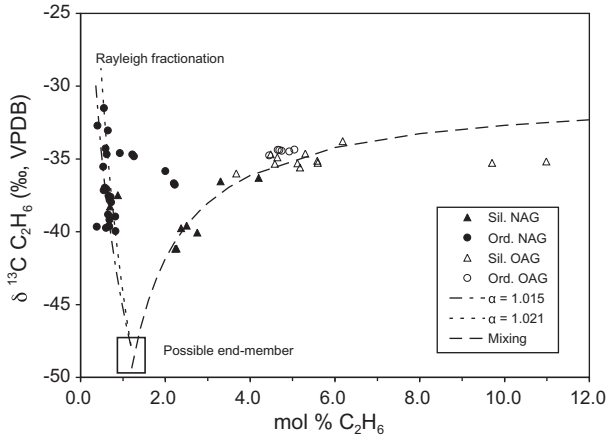

Fig. 10. Mixing and Rayleigh fractionation replotted with linear concentration scale. The mixing curve is now hyperbolic (Kendall and Caldwell, 1998) between OAG with about 12 mol% ethane and NAG with about 1.2 mol% ethane and Rayleigh-type fractionation starting 1.2 mol% ethane with $\delta^{13}C_2 = -48‰$ and fractionation factors expressed in per mil at 200 °C and 300 °C (Tang et al., 2000).

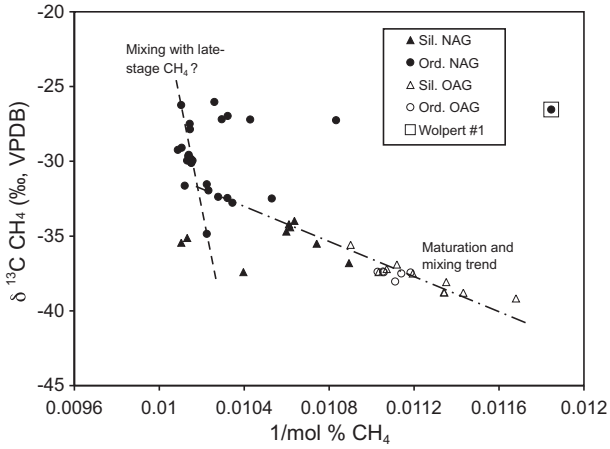

Fig. 11. Variation of methane isotopic composition with concentration. The maturation and mixing trend (dash-dot line to guide the eye) includes gases in the shallowest OAG in Silurian age reservoirs and shallower NAG in Silurian and Ordovician age reservoirs. These points fall along the maturation trend on the Schoell plot (Fig. 4). A possible second mixing trend (dashed line to guide the eye) in the deepest NAG is consistent with the trend on the Schoell plot that extends to a hypothetical "late-stage CH_4". The sample that deviates the most from these trends is the Wolpert #1 well (within box) that contains measureable H_2S. Methane concentration and isotopic composition in this sample may be affected by TSR. See text for discussion.

or:

$$4C_2H_6 = 2C + 6CH_4 \quad (3)$$

The isotopic composition of the residual ethane is controlled by KIEs (Hayes, 2001) and the magnitude of the KIE at any temperature is controlled by bond energies (Tang et al., 2000). The extent of fractionation of the residual gas can be modeled as a Rayleigh-type process (Rooney, 1995). *Ab initio* calculated fractionation factors for ethane and propane loss at 200–300 °C will generate the observed isotopic compositions by destruction of 60–70% of the initial concentration of the gas (Fig. 9B). For Rayleigh-type fractionation to be the dominant control on the isotopic composition, the system must contain a finite amount of ethane and propane that is not replenished by continued generation in source rocks. The fact that only NAG show evidence of Rayleigh-type fractionation implies that a gas source from late stage oil cracking is not present, probably because oil cracking has gone to completion. This is consistent with experiments on gas generation from thermally mature organic matter (Lorant and Behar, 2002) and with observations of pyrobitumen in these reservoirs (Laughrey and Kostelnik, 2007).

Redox reactions dominated by Fe^{2+}/Fe^{3+} appear to control the abundance of CO_2 and light hydrocarbon gases in geothermal systems (Gherardi et al., 2005; Giggenbach, 1987). In systems where the concentrations of ethane and propane are abundant enough to allow isotopic analysis (Des Marais et al., 1981) partial reversals are observed. Recent work on Italian geothermal systems (Gherardi et al., 2005) shows one system with a normal ^{13}C sequence and two systems with $\delta^{13}C_1 > \delta^{13}C_2$. A recent experimental study (Pan et al., 2006) examined the molecular and isotopic changes in hydrocarbon gases by oxidation reactions with sulfur species and magnetite and hematite. The isotopic shifts observed are similar to those we observe, but the magnitudes are not consistent with a Rayleigh fractionation model.

4.2.2. Late stage methane reactions

In contrast to the changes in ethane and propane isotopic compositions, the methane isotopic composition appears to be dominated by mixing with late stage methane that is enriched in ^{13}C but depleted in ^{2}H (Fig. 4). One mechanism than can cause ^{2}H depletion in CH_4 is isotopic exchange of hydrogen with formation water. Fractionation factors calculated for temperatures of 200–300 °C that are based on exchange experiments between water and methane (Horibe and Craig, 1995) indicate that δ^2H in methane should be depleted by −143‰ to −125‰ relative to coexisting water. Palaeozoic brines from oil and gas reservoirs in Pennsylvania and Ohio have δ^2H values of −30‰ to −40‰ (Breen et al., 1985; Dresel, 1985). Methane equilibrated with water of this composition at temperatures of maximum burial in the Appalachian basin will have δ^2H compositions of about −183‰ to −160‰, well within the range needed for a possible end member. Hydrogen isotope exchange between water and methane has been observed in geothermal gases, but not reported before for natural gas accumulations. Recently published experimental work (Seewald et al., 2006) provides additional evidence for hydrogen isotopic exchange between methane and water.

In deeply buried parts of the Appalachian basin that underwent metamorphism, late stage methane generation could occur in carbonaceous metasediments through reactions documented in metamorphic rocks (Burruss, 1993) such as:

$$2C + 2H_2O = CH_4 + CO_2 \quad (4)$$

Given the low CO_2 content (<1.5 mol%, with most <0.5 mol%, Fig. 8C) of these gases, reaction (4) alone cannot be the dominant source of late stage methane without loss of most of the co-generated CO_2. However, at the depths and temperatures of maximum burial in the Appalachian basin, the carbonaceous material will be residual kerogen or pyrobitumen from oil cracking and not pure graphite. If the H/C ratio of solid organic matter is on the order of 0.2 (approximately the ratio at anthracite coal rank), then reaction (4) can be rewritten as:

$$C_{20}H_4 = 19C + CH_4 \quad (5)$$

$$C_{20}H_4 + 2H_2O = 17C + 2CH_4 + CO_2 \quad (6)$$

causing a lower and variable ratio of CH_4 to CO_2 rather than a 1:1 ratio required by reaction (4).

If a redox couple is present, then reaction (7) in which C represents residual kerogen or pyrobitumen

$$C + 2H_2O + 4Fe_3O_4 = 3Fe_2O_3 + CH_4 \quad (7)$$

could generate late stage methane. As written, reaction (7) is a reaction in which water is reduced by Fe^{2+} to yield hydrogen that can react with residual carbonaceous material to form methane.

Although evidence for isotopic exchange between CH_4 and H_2O has been discussed in hydrothermal systems, we believe our observations provide the first possible evidence for hydrogen isotopic exchange between CH_4 and H_2O in commercial natural gas accumulations. Although we know that hydrogen isotopic exchange between hydrocarbons and water occurs in nature (Schimmelmann et al., 2006), it is clear that the alkanes are the most resistant to exchange (Schimmelmann et al., 2006) and methane should be the least reactive alkane. However, we also know from experimental studies to measure equilibrium isotopic exchange factors that exchange is facilitated by chemical reactions that involve the molecular species involved in the isotopic exchange (Cole and Chakraborty, 2001). Therefore, if the water–rock–gas environment during deep basin burial can drive reactions such as 1, 2, 4, 6, or 7 that involve methane and water, there should be a high potential for isotopic exchange.

4.3. Origin and implications of isotopic reversals in natural gas

4.3.1. Gases in the deep Appalachian basin

Two processes, mixing and Rayleigh-type fractionation, appear to be responsible for the isotopic reversals observed in the deep Appalachian basin. Although mixing has been proposed as the cause of partial reversals observed in previous work in the Appalachian basin (Jenden et al., 1993; Laughrey and Baldassare, 1998) we cannot make an internally consistent mixing model using only the compositions of the NAG and OAG to reproduce the complete reversals we observe. This is due to the fact that the observed isotopic composition of ethane does not change monotonically with molecular concentration (Fig. 10). An end member with an intermediate concentration of isotopically light ethane is required. Isotopically light *G. prisca* rich organic matter is the probable source of that end member gas that is consistent with the geologic setting of the samples. This end member gas is then fractionated by Rayleigh-type processes that destroy ethane and propane, driving the isotopic compositions of the components to progressively heavier values. Rayleigh-type fractionation can cause isotopic fractionation only in systems that have an initial fixed concentration of the component being fractionated. If ethane is continuously replenished by cracking of higher hydrocarbons at the same time it is cracking or being oxidized, a steady state isotopic composition would be attained, not progressively heavier compositions. This appears to be the case in the deep Appalachian basin because all of the NAG are truly non-associated. No higher hydrocarbon liquids are present that could crack to small molecules and continuously generate ethane.

Methane in the deepest reservoirs with $\delta^{13}C$ and $\delta^{2}H$ that plot on mixing trend 2 (Fig. 4) clearly requires a source of gas that is isotopically enriched in ^{13}C, commonly called "super mature" methane, but which is isotopically depleted in ^{2}H. This could be late stage methane generated from more deeply buried Utica Shale that has undergone the initial stages of metamorphism that has equilibrated with formation water during tectonic burial during the Alleghanian orogeny.

Burial history modeling of the deepest part of the Appalachian basin beneath the eastern margin of the fold and thrust belt (Rowan, 2006) shows that Ordovician age source rocks reached the oil window before accumulation of thrust sheets during Alleghanian deformation. Therefore hydrocarbon liquids and gases with a range of isotopic compositions generated from different organic matter facies within the source rock could have mixed during accumulation in traps beneath the Alleghanian foreland sediments. As the Alleghanian orogeny continued, thrust sheets overrode the thickest sequence of pre-Devonian sediments, pushing source rocks and previously accumulated hydrocarbons to depths of 10–12 km. At the maximum temperatures of burial, the higher hydrocarbons were cracked and residual ethane and propane were progressively destroyed, causing isotopic compositions to shift to heavier values through Rayleigh fractionation. Late stage methane re-equilibrated with formation water and mixed with residual accumulations of hydrocarbon gases.

Although we are invoking multiple stages of hydrocarbon generation and migration to drive the mixing and alteration processes required to explain isotopic reversals, this not uncommon in foreland fold-and-thrust belts like the Appalachian Basin. Furthermore, there are a number of fluid inclusion studies that document multiple stages of migration of hydrocarbons and formation waters during deformation of the Appalachian basin (Evans and Battles, 1999; O'Reilly and Parnell, 1999; Harrison et al., 2004; Cook et al., 2006; O'Kane et al., 2007; Onasch et al., 2009) including methane-rich gas migration in Ordovician age rocks that underwent the initial stages of burial metamorphism (Kisch and van den Kerkhof, 1991) in the deeply buried part of the basin.

4.3.2. Comparison with other deep basin gas accumulations

If our explanation of progressive depletion of ^{12}C in ethane and propane through redox reactions is correct, then isotopic reversals of these gases may be evidence of limits to the stability of hydrocarbon gases in sedimentary basins. Partial reversals are observed in gases in the deep Rotliegendes Basin with $\delta^{13}C_1 < \delta^{13}C_2$ and $\delta^{13}C_2 > \delta^{13}C_3$ and $\delta^{13}C_2 = -17$ to -21 (Mueller and Schulz, 2004). Methane and ethane isotopic compositions are heavier than we observe and not reversed but may also be evidence of resource limitation by redox reactions. Natural gas plots to estimate the isotopic composition of the source material always yield isotopic compositions that are much heavier ($\delta^{13}C > -20‰$) than any possible source material. This suggests that Rayleigh fractionation during deep burial is driving the isotopic compositions of all the hydrocarbon gases, including methane, to heavier values. In this case, all the hydrocarbon gases are being destroyed by fluid–rock reactions, suggesting that deeper, economic accumulations of natural gas are unlikely.

5. Conclusions

We have documented complete reversals in the normal trend of carbon isotopic composition of methane, ethane and propane in NAG in the deepest reservoirs of Silurian and Ordovician age in the northern Appalachian basin. OAG and NAG in shallower reservoirs are not reversed or only partially reversed. The ^{13}C and ^{2}H compositions of methane in OAG and shallow NAG are consistent with generation of gases from middle Ordovician age source rocks that have isotopic compositions that span the full range of isotopic compositions observed in rocks of this age. The ^{2}H compositions of methane show a reversal in the normal trend of enrichment with increasing depth to a trend of progressive depletion with depth. The ^{2}H compositions of methane and ethane in OAG and NAG are also reversed.

Using a combination of mixing of gases and Rayleigh fractionation models, we have modeled the isotopic compositions of gases across the full range of normal to fully reversed isotopic compositions. Rayleigh-type fractionation of the higher hydrocarbons requires processes that destroy these components. We have proposed that these reactions involve redox reactions with transition metals and water at late stages of diagenesis at temperatures on the order of 250–300 °C. *Ab initio* calculated fractionation factors for C–C bond breaking in ethane at these temperatures are consistent with the observed variations in concentration and carbon isotopic composition. The reversal in the ^{2}H composition of methane can be explained by mixing with a late stage, super mature methane that has isotopically exchanged with formation water at these temperatures.

Our interpretation that Rayleigh fractionation during redox reactions is causing isotopic reversals has important implications for natural gas resources in deeply buried sedimentary basins. In this scenario isotopic reversals between ethane and propane are a signal that all higher hydrocarbons have been depleted from the petroleum system. In the case of the Appalachian basin described here, there appears to be addition of late stage methane to the system that may be important for the economic resource potential in the deep basin. However, in other deep basins, such as the Rotliegendes, isotopically heavy gases, with partial reversals may be indicating progressive loss of all hydrocarbon gases including methane.

In any case, unraveling the complex processes that create and limit the size of natural gas resources in deep basins will require detailed, compound specific isotopic analyses of the gases using both ^{13}C and ^{2}H. Those observations, combined with molecular analysis, provide the maximum amount of information available to interpret the history of hydrocarbon accumulation and the resource potential for natural gas in deep basins.

Acknowledgements

This work was supported by the USGS Petroleum Processes Project and the National Oil and Gas Assessment Project (RCB) and by US DOE/NETL (Award Number DE-FC26-03NT41856), an industry-funded grant, and the Pennsylvania Geological Survey (CDL). Many individuals at independent oil and gas exploration and production companies and state geological surveys provided critical assistance in sample collection. Michael Trippi assisted with preparation of Fig. 1. Martin Schoell, Michael Bikerman, Peter Warwick and Sean Brennan commented on an early draft of this manuscript. Comments and suggestions by Darius Strapoc and an anonymous reviewer were very helpful in improving the consistency of the presentation and discussion of this work. Use of commercial trade names does not constitute endorsement by the US Geological Survey or the Pennsylvania Geological Survey.

Associate Editor—**Simon George**

References

Barker, J.F., Pollock, S.J., 1984. The geochemistry and origin of natural gases in southern Ontario. Bulletin of Canadian Petroleum Geology 32, 313–326.

Behar, F., Kressmann, S., Rudkiewicz, J.L., Vandenbroucke, M., 1992. Experimental simulation in a confined system and kinetic modelling of kerogen and oil cracking. Organic Geochemistry 19, 173–189.

Bernard, B.B., Brooks, J.M., Sackett, W.M., 1976. Natural gas seepage in the Gulf of Mexico. Earth and Planetary Science Letters 31, 48–54.

Berner, U., Faber, E., Scheeder, G., Panten, D., 1995. Primary cracking of algal and landplant kerogens: kinetic models of isotope variations in methane, ethane, and propane. Chemical Geology 126, 233–245.

Bottinga, Y., 1969. Calculated fractionation factors for carbon and hydrogen isotope exchange in the system calcite–carbon dioxide–graphite–methane–hydrogen–water vapor. Geochimica et Cosmochimica Acta 33, 49–64.

Breen, K.J., Angelo, C.G., Masters, R.W., Sedam, A.C., 1985. Chemical and isotopic characteristics of brines from three oil- and gas-producing sandstones in eastern Ohio, with applications to the geochemical tracing of brine sources. US Geological Survey Water-Resources Investigations Report 84-4314, 63 p.

Burruss, R.C., 1993. Stability and flux of methane in the deep crust – a review. In: Howell, D.G. (Ed.), The Future of Energy Gases, US Geological Survey Professional Paper 1570, pp. 21–29.

Burruss, R.C., Ryder, R.T., 2003. Composition of crude oil and natural gas produced from 14 wells in the Lower Silurian "Clinton" sandstone and Medina Group, northeastern Ohio and northwestern Pennsylvania, US Geological Survey Open File Report 03-409, 64 p.

Chung, H.M., Gormly, J.R., Squires, R.M., 1988. Origin of gaseous hydrocarbons in subsurface environments: theoretical considerations of carbon isotope distribution. Chemical Geology 71, 97–103.

Cole, D.R., Chakraborty, S., 2001. Rates and mechanisms of isotopic exchange. In: Valley, J.W., Cole, D.R. (Eds.), Stable Isotope Geochemistry, Reviews in Mineralogy and Geochemistry 43, pp. 83–191.

Cook, J.E., Dunne, W.M., Onasch, C.M., 2006. Development of a dilatant damage zone along a thrust relay in a low-porosity quartz arenite. Journal of Structural Geology 28, 776–792.

Dai, J., Xia, X., Qin, S., Zhao, J., 2004. Origins of partially reversed alkane $\delta^{13}C$ values for biogenic gases in China. Organic Geochemistry 35, 405–411.

Dennen, K.O., Deering, M., Burruss, R.C., 2007. The geochemistry of oils and gases from the Cumberland Overthrust Block in Virgnia and Tennessee. In: Ruppert, L. (Ed.), Coal and Petroleum Resources in the Appalachian Basin: Distribution, Geologic Framework, and Geochemical Character, US Geological Survey Professional Paper 1708, pp. 220-242.

Des Marais, D.J., Donchin, J.H., Nehring, N.L., Truesdell, A.H., 1981. Molecular carbon isotopic evidence for the origin of geothermal hydrocarbons. Nature 292, 826–828.

Dresel, P.E., 1985. The geochemistry of oilfield brines from western Pennsylvania. M.S. disseration, Department of Geosciences, The Pennsylvanian State University. State College. PA 168 p..

Evans, M.A., Battles, D.A., 1999. Fluid inclusion and stable isotope analyses of veins from the central Appalachian Valley and Ridge Province; implications for regional synorogenic hydrologic structure and fluid migration. Geological Society of American Bulletin 111, 1841–1860.

Gherardi, F., Panichi, C., Gonfiantini, R., Magro, G., Scandiffio, G., 2005. Isotope systematics of C-bearing gas compounds in the geothermal fluids of Lardarello, Italy. Geothermics 35, 442–470.

Giggenbach, W.F., 1987. Redox processes governing the chemistry of fumarolic gas discharges from White Island, New Zealand. Applied Geochemistry 2, 143–161.

Harrison, M.J., Marshak, S., Onasch, C.M., 2004. Stratigraphic control of hot fluids on anthracitization, Lackawanna synclinorium, Pennsylvania. Tectonophysics 378, 85–103.

Hatch, J.R., Jacobson, S.R., Witzke, B.J., Rissatti, J.B., Anders, D.E., Watney, W.L., Newell, K.D., Vuletich, A.K., 1987. Possible late Middle Ordovician organic carbon isotope excursion: evidence from Ordovician oil and hydrocarbon source rocks, mid-continent and east-central United States. American Association of Petroleum Geologists Bulletin 71, 1342–1354.

Hayes, J.M., 2001. Fractionation of carbon and hydrogen isotopes in biosynthetic processes. In: Valley, J.W., Cole, D.R. (Eds.), Stable Isotope Geochemistry, Reviews in Mineralogy and Geochemistry 43, pp. 225–318.

Horibe, Y., Craig, H., 1995. D/H fractionation in the system methane–hydrogen–water. Geochimica et Cosmochimica Acta 59, 5209–5217.

Huang, H., Yang, J., Yang, Y., Du, X., 2004. Geochemistry of natural gases in deep strata of the Songliao basin, NE China. International Journal of Coal Geology 58, 231–244.

Hulston, J.R., Hilton, D.R., Kaplan, I.R., 2001. Helium and carbon isotope systematics of natural gases from Taranaki Basin, New Zealand. Applied Geochemistry 16, 419–436.

Hunt, J.M., 1996. Petroleum Geochemistry and Geology. W.H. Freeman and Company, New York. 743 p.

James, A.T., 1983. Correlation of natural gas by use of carbon isotopic distribution between hydrocarbon components. American Association of Petroleum Geologists Bulletin 67, 1176–1191.

James, A.T., Burns, B.J., 1984. Microbial alteration of subsurface natural gas accumulations. American Association of Petroleum Geologists Bulletin 68, 957–960.

Jenden, P.D., Drazan, D.J., Kaplan, I.R., 1993. Mixing of thermogenic natural gases in northern Appalachian basin. American Association of Petroleum Geologists Bulletin 77, 980–998.

Kendall, C., Caldwell, E.A., 1998. Fundamentals of isotope geochemistry. In: Kendall, C., McDonnell, J.J. (Eds.), Isotope Traces in Catchment Hydrology. Elsevier, New York, pp. 51–86.

Kisch, H.J., van den Kerkhof, A.M., 1991. CH_4-rich inclusions form quartz veins in the Valley-and-Ridge province and the anthracite fields of the Pennsylvania Appalachians. American Mineralogist 76, 230–240.

Krouse, H.R., Viau, C.A., Eliuk, A.L.S., Ueda, S., Halas, S., 1988. Chemical and isotopic evidence of thermochemical sulfate reduction by light hydrocarbon gases in deep carbonate reservoirs. Nature 333, 415–419.

Laughrey, C.D., Baldassare, F.J., 1998. Geochemistry and origin of some natural gases in the Plateau province of the central Appalachian basin, Pennsylvania and Ohio. American Association of Petroleum Geologists Bulletin 82, 317–335.

Laughrey, C.D., Harper, R.M., 1996. Upper Ordovician Bald Eagle Formation fractured anticlinal play. In: Roen, J.B., Walker, B.J. (Eds.), The atlas of major Appalachian gas plays, West Virginia Geological and Economic Survey Publication V-25, pp. 164–167.

Laughrey, C.D., Kostelnik, J., 2007. Geochemistry of natural gases from Trenton and Black River Formation (Middle Ordovician) Carbonate Reservoirs, Appalachian Basin. In: Patchen, D.G., Hickman, J.B., Harris, D.C., Drahovzal, J.A. (Eds.), Final Report: A Geologic Play Book for Trenton-Black River Appalachian Basin Exploration, US Department of Energy Award Number DE-FC26-03NT41856, Department of Energy/National Energy Technology Laboratories, pp. 161–210.

Lewan, M.D., 1997. Experiments on the role of water in petroleum formation. Geochimica et Cosmochimica Acta 61, 3671–3723.

Lorant, F., Behar, F., 2002. Late generation of methane from mature kerogens. Energy & Fuels 16 (2), 412–427.

Lorant, F., Prinzhofer, A., Behar, F., Huc, A.-Y., 1998. Carbon isotopic and molecular constraints on the formation and the expulsion of thermogenic hydrocarbon gases. Chemical Geology 147, 249–264.

Mastalerz, M., Schimmelmann, A., Hower, J.C., Lis, G., Hatch, J.R., Jacobson, S.R., 2003. Chemical and isotopic properties of kukersites from Iowa and Estonia. Organic Geochemistry 34, 1419–1427.

Mueller, E., Schulz, T., 2004. Application of geochemistry in the evaluation and development of deep Rotliegend dry gas reservoirs, NW Germany. In: Cubitt, J.M., England, W.A., Larter, S. (Eds.), Understanding Petroleum Reservoirs: Towards an Integrated Reservoir Engineering and Geochemical Approach, Special Publication 237. Geological Society of London, pp. 221–230.

O'Kane, A., Onasch, C.M., Farver, J.R., 2007. The role of fluids in low temperature, fault-related deformation of quartz arenite. Journal of Structural Geology 29, 819–836.

Onasch, C.M., Dunne, W.M., Cook, J.E., O'Kane, A., 2009. The effect of fluid composition on the behavior of well cemented, quartz-rich sandstone during faulting. Journal of Structural Geology 31, 96–971.

O'Reilly, C., Parnell, J., 1999. Fluid flow and thermal histories for Cambrian–Ordovician platform deposits, New York: evidence from fluid inclusion studies. Geological Society of America Bulletin 111, 1884–1896.

Pan, C., Yu, L., Fu, J., 2006. Chemical and carbon isotopic fractionations of gaseous hydrocarbons during abiogenic oxidation. Earth and Planetary Science Letters 246, 70–89.

Patchen, D.G., Hickman, J.B., Harris, D.C., Drahovzal, J.A., Lake, P.D., Smith, L.B., Nyahay, R., Schulze, R., Riley, R.A., Baranowski, M.T., Wickstrom, L.H., Laughrey, C.D., Kostelnik, J., Harper, R.M., Avary, K.L., Bocan, J., Hohn, M.E., McDowell, R., 2006. A geologic play book for Trenton-Black River Appalachian basin exploration, US Department of Energy, 632 p.

Prinzhofer, A., Huc, A.Y., 1995. Genetic and post-genetic molecular and isotopic fractionations in natural gases. Chemical Geology 126, 281–290.

Proskurowski, G., Lilley, M.D., Seewald, J.S., Fruh-Green, G.L., Olson, E.J., Lupton, J.E., Sylva, S.P., Kelley, D.S., 2008. Abiogenic hydrocarbon production at Lost City hydrothermal field. Science 319, 604–607.

Repetski, J.E., Ryder, R.T., Weary, D.J., Harris, A.G., Trippi, M.H., 2008. Thermal maturity patterns (CAI and %R_o) in upper Ordovician and Devonian rocks of the Appalachian basin: a major revision of USGS Map I-917-E using new subsurface collections. US Geological Survey Scientific Investigations Map 3006, 30 p.

Rooney, M.A., Claypool, G.E., Chung, H.M., 1995. Modeling thermogenic gas generation using carbon isotope ratios of natural gas hydrocarbons. Chemical Geology 126, 219–232.

Rowan, E.L., 2006. Burial and thermal history of the central Appalachian basin, based on three 2-D models of Ohio, Pennsylvania, and West Virginia. US Geological Survey Open File Report 2006-1019, 37 p.

Ryder, R.T., Zagorski, W.A., 2003. Nature, origin, and production characteristics of the Lower Silurian regional oil and gas accumulation, central Appalachian basin, United States. American Association of Petroleum Geologists Bulletin 87, 847–872.

Ryder, R.T., Burruss, R.C., Hatch, J.R., 1998. Black shale source rocks and oil generation in the Cambrian and Ordovician of the Central Appalachian Basin, USA. The American Association of Petroleum Geologists Bulletin 82, 412–441.

Schimmelmann, A., Sessions, A.L., Mastalerz, M., 2006. Hydrogen isotopic composition (D/H) of organic matter during diagenesis and thermal maturation. Annual Reviews of Earth and Planetary Science 34, 501–533.

Schoell, M., 1983. Genetic characterization of natural gases. American Association of Petroleum Geologists Bulletin 67, 2225–2238.

Schumaker, R.C., 1996. Structural history of the Appalachian basin. In: Roen, J.B., Walker, B.J. (Eds.), The atlas of major Appalachian gas plays, West Virginia Geological and Economical Survey Publication V-25, pp. 8–21.

Seewald, J.S., Zolotov, M.Y., McCollom, T., 2006. Experimental investigation of single carbon compounds under hydrothermal conditions. Geochimica et Cosmochimica Acta 70, 446–460.

Sherwood Lollar, B., Westgate, T.D., Ward, J.A., Slater, G.F., Lacrampe-Couloume, G., 2002. Abiogenic formation of alkanes in the Earth's crust as a minor source for global hydrocarbon reservoirs. Nature 416, 522–524.

Sherwood Lollar, B., Lacrampe-Couloume, G., Slater, G.F., Ward, J.A., Moser, D.P., Gihring, T.M., Lin, L.-H., Onstott, T.C., 2006. Unraveling abiogenic and biogenic sources of methane in the earth's deep subsurface. Chemical Geology 226, 328–339.

Sherwood Lollar, B., Lacrampe-Couloume, G., Voglesonger, K., Onstott, T.C., Pratt, L.M., Slater, G.F., 2008. Isotopic signatures of CH_4 and higher hydrocarbon gases from Precambrian Shield sites: a model for abiogenic polymerization of hydrocarbons. Geochimica et Cosmochimica Acta 72, 4778–4795.

Swezey, C.S., 2002. Regional stratigraphy and petroleum systems of the Appalachian basin, North America. US Geological Survey Geologic Investigations Series Map I-2768.

Tang, Y., Perry, J.K., Jenden, P.D., Schoell, M., 2000. Mathematical modeling of stable carbon isotope ratios in natural gases. Geochimica et Cosmochimica Acta 64, 2673–2687.